REPORT DOCUMENTATION PAGE

Form Approved
OMB No. 0704-0188

1. REPORT DATE *(DD-MM-YYYY)*	2. REPORT TYPE	3. DATES COVERED *(From - To)*
12-06-2007	Conference Proceedings	

4. TITLE AND SUBTITLE
Wave Measurements Using a Dual-beam Interferometer Near Gulf Stream Boundary

5a. CONTRACT NUMBER

5b. GRANT NUMBER

5c. PROGRAM ELEMENT NUMBER
PE061153N & PE062435

6. AUTHOR(S)
Paul A. Hwang, Jakov Toporkov, Mark Sletten, Douglas Lamb, Dragana Perkovic

5d. PROJECT NUMBER

5e. TASK NUMBER

5f. WORK UNIT NUMBER
73-6628-06-5

7. PERFORMING ORGANIZATION NAME(S) AND ADDRESS(ES)
Naval Research Laboratory
Oceanography Division
Stennis Space Center, MS 39529-5004

8. PERFORMING ORGANIZATION REPORT NUMBER
NRL/JA/7330-06-6191

9. SPONSORING/MONITORING AGENCY NAME(S) AND ADDRESS(ES)
Office of Naval Research
800 N. Quincy St.
Arlington, VA 22217-5660

10. SPONSOR/MONITOR'S ACRONYM(S)
ONR

11. SPONSOR/MONITOR'S REPORT NUMBER(S)

12. DISTRIBUTION/AVAILABILITY STATEMENT
Approved for public release, distribution is unlimited.

13. SUPPLEMENTARY NOTES

14. ABSTRACT
A dual-beam interferometric synthetic aperture radar provides two velocity components of the ocean current remotely from a single fight pass. Combining two flight passes, all three orthogonal components of the surface velocity can be retrieved. An experiment was conducted near the Gulf Stream (GS) boundary. A sharp change of the surface velocity of about 1 m/s over a 500 m distance was measured. The wave condition is dominated by a 14-s swell system and low wind velocity. The wave variance inside GS is about twice the wave variance outside the GS in the present data. The large difference in the wave variance is considerably higher than that can be expected from hydrodynamic modulation. An ocean current system with strong current shears such as the Gulf Stream is a wave guide and can trap waves with the right combination of wavelengths and propagation directions. Numerical calculations indicate that the wave properties of the data set may satisfy the conditions for wave trapping by the Gulf Stream.

15. SUBJECT TERMS
Surface waves, Gulf Stream, InSAR, wave guide, wave modulation

16. SECURITY CLASSIFICATION OF:			17. LIMITATION OF ABSTRACT	18. NUMBER OF PAGES	19a. NAME OF RESPONSIBLE PERSON
a. REPORT	b. ABSTRACT	c. THIS PAGE			Paul Hwang
Unclassified	Unclassified	Unclassified	UL	4	19b. TELEPHONE NUMBER *(Include area code)* 202-767-0800

Wave measurements using a dual-beam interferometer near Gulf Stream boundary

Paul A. Hwang[1], Jakov V. Toporkov[1], Mark A. Sletten[1], Douglas Lamb[1], and Dragana Perkovic[2]

[1] Naval Research Laboratory, 4555 Overlook Ave. SW, Washington DC 20375 USA

[2] University of Massachusetts, Amherst, MA 01003 USA

***Abstract*–A dual-beam interferometric synthetic aperture radar yields two velocity components of the ocean current remotely from a single flight pass. Combining two flight passes, all three orthogonal components of the surface velocity can be retrieved. An experiment was conducted near the Gulf Stream (GS) boundary. A sharp change of the surface velocity of about 1 m/s over a 500 m distance was measured. The wave condition is dominated by a 14-s swell system and low wind velocity. The wave variance inside GS is about twice of the wave variance outside the GS in the present data set. The large difference in the wave variance is considerably higher than that can be expected from hydrodynamic modulation. An ocean current system with strong current shears such as the Gulf Stream is a wave guide and can trap waves with the right combinations of wavelengths and propagation directions. Numerical calculations indicate that the wave properties of the data set may satisfy the conditions for wave trapping by the Gulf Stream.**

Keywords- Surface waves, Gulf Stream, InSAR, Wave guide, Wave modulation

I. INTRODUCTION

An along-track interferometric synthetic aperture radar (InSAR) can measure the near-surface ocean currents remotely by detecting the phase difference of the radar returns from the same ocean surface roughness using two receiving antennas mounted on an aircraft or satellite [1-3]. The phase difference between the received signals from the two antennas is produced by the Doppler frequency shift caused by the ocean current advecting the surface waves that scatter the radar signals back to the receivers. To the first order of approximation, the phase shift is proportional linearly to the velocity component projected in the range direction. With proper design, the InSAR can yield sufficient spatial resolution for surface wave measurements [4-7]. The relationship between surface waves and the InSAR velocity product is much more straightforward than the modulation transfer function associating the surface waves and the SAR signal amplitude [8-9]. Because distortion of the waveform through the velocity bunching mechanism remains in the InSAR measurements, reliable retrieval of the wave information from InSAR is still limited by the nonlinearity of the wave field.

In the side-looking InSAR, only one radial velocity in the radar range direction can be measured. To obtain the vector field of the ocean current, multiple passes through the same ocean surface area have to be conducted. The concept of deriving two velocity components from the InSAR return by splitting the radar beams was described in [10]. A design employs two pairs of antennas placed with two different squint angles, one pair looking fore and one pair aft, and each pair serves as an InSAR system [11]. The images from the two pairs (fore and aft) are then geo-collocated to yield the velocity vector of the ocean surface in a single flight pass. The description of the system, called a dual-beam interferometer (DBI), has been given in [12] and [13], the latter paper also reported an application of the DBI to map out the velocity field around two tidal inlets in the barrier islands west of Fort Myers, Florida. The retrieved current field follows the outflow pattern expected from the geometry of the barrier islands and the inlets. Comparisons with the tidal current magnitudes predicted by the U. S. National Ocean Service reveal discrepancies of up to 0.5 m/s. Their analyses suggest that an important factor contributing to the discrepancies is the effect of ocean surface waves to the overall InSAR velocity measurement.

Because surface waves affect the accuracy of the surface current derivation from InSAR, and that wave information is contained in the InSAR data, in this paper, we investigate the computation of surface wave spectrum using the DBI measurements. In the process, it is found that for this data set of swell-dominated wave field, the difference of the variance inside and outside the Gulf Stream (GS) is much larger than that can be explained by current modulation of surface waves. Further analysis suggests that a more likely explanation of the observed large wave variance inside the GS is due to wave trapping. That is, the wave properties of the acquired data set satisfy the conditions for the GS to serve as a wave guide.

II. DBI MEASUREMENTS NEAR GULF STREAM BOUNDARY

In March 2004, an experiment was conducted to test the DBI system. The general location of the experiment is offshore of Cape Canaveral, Florida. Two NDBC buoys (41009 – 15 km from DBI site; and 41010 – 145 km from DBI site) are nearby and provide the pertinent environmental information including wind velocity, air and water temperature, and wave properties. The surface area of the DBI coverage is about 2.8 km × 10 km. A couple of high-wind events passed through the area in the week before data acquisition. The event on 10 to 11 March had sustained wind speeds between 10 and 12 m/s and lasted for about 16 hours. The weather system continued moving eastward and at the time of DBI experiment more than one day later, the significant wave height at the offshore buoy site (41010, water depth 873 m) is almost 5 m although the wind speed dropped to below 5 m/s in both buoy locations. The significant wave height in the nearshore site (41009) is about one-half of the offshore magnitude. The peak wave periods reported by the two buoys are 14.29 s (41010) and 13.79 s (41009, water depth 41.5 m) at the time of DBI measurements.

A detailed analysis of the DBI design is given in [11]. The DBI system configurations used in the present experiment have been reported elsewhere [12-13]. Briefly, the DBI operates at C-band (5.3 GHz) and vertical polarization. It emits a 6.25-μs-long chirp signal with a 25-MHz bandwidth that provides a 6-m range resolution. The squint angles of the fore- and aft-looking antenna pairs are nominally +20° and -20°, respectively. The physical baseline in each pair is 1.23 m, only the fore-looking antenna in each pair transmits. The antennas point at a 70° incident angle in their squinted planes. The antenna patterns are broad in elevation (31°) and narrow in azimuth (7°). The aircraft speed is 100 m/s and the altitude 600 m. The range of incident angles is between 50.3° and 80.6°.

III. DATA PROCESSING

The radial velocity components, u_1 and u_2, in the two squint directions are related to the phases, Φ_1 and Φ_2, by [*Frasier and Camps*, 2001; *Toporkov et al.*, 2005]

$$u_j = \frac{\Phi_j}{4\pi}\frac{\lambda}{B_e}V_p, \qquad j=1, 2, \tag{1}$$

where λ is the radar wavelength, V_p the platform speed, and B_e the effective baseline, which is one-half of the physical along-track antenna separation because only one antenna in each pair is transmitting. With the present configurations, for the full range of the phase ($\pm\pi$), the magnitude of current without wraparound ambiguity is ±2.30 m/s. The raw processed phase data contain an arbitrary offset, which can be removed if there are fixed objects in the images for reference. This is not the case in the present situation. The aircraft made repeated passes over the region, the time interval between two consecutive passes is about 600 s. Feature tracking is applied to estimate the velocities of several slick-like features in the radar scatter amplitude maps in consecutive passes. The features in the inshore side of the GS usually maintain their coherent characteristics during the two passes and are easy to identify. Features inside the GS are distorted beyond recognition in two consecutive passes, therefore, velocity estimates from feature tracking are only available for the inshore side of the GS front. The average velocity amplitude and direction of five identifiable features is 0.82 m/s and 103° (referenced to east). This average velocity is used in data processing to determine the offset of the measured radar phase.

Following the notations and geometry defined in Fig. 1 of [13] and assuming that the current is confined to the horizontal plane, the surface velocity components can be calculated from the radial components

$$\begin{aligned} v_x &= \frac{u_1\cos\theta_{s2} - u_2\cos\theta_{s1}}{\sin(\theta_{s1}-\theta_{s2})} \\ v_y &= \frac{u_2\sin\theta_{s1} - u_1\sin\theta_{s2}}{\sin(\theta_{s1}-\theta_{s2})\sin\theta_i} \end{aligned}, \tag{2}$$

Combining two flight passes, the assumption of v_z=0 for the above solution can be discarded, and all three orthogonal components of the surface velocity can be derived from the radial velocity measurements.

$$\begin{bmatrix} u_1 \\ u_2 \\ u_3 \end{bmatrix} = \begin{bmatrix} \sin\theta_{s1} & \cos\theta_{s1}\sin\theta_{i1} & -\cos\theta_{s1}\cos\theta_{i1} \\ \sin\theta_{s2} & \cos\theta_{s2}\sin\theta_{i2} & -\cos\theta_{s2}\cos\theta_{i2} \\ b_{31} & b_{32} & b_{33} \end{bmatrix} \begin{bmatrix} v_x \\ v_y \\ v_z \end{bmatrix} \tag{3}$$

where $b_{31}=\sin\theta_{s3}\cos\alpha_3$ - $\cos\theta_{s3}\sin\theta_{i3}\sin\alpha_3$, $b_{32}=\sin\theta_{s3}\sin\alpha_3$ - $\cos\theta_{s3}\sin\theta_{i3}\cos\alpha_3$, and $b_{33}=\cos\theta_{s3}\sin\theta_{i3}$. The above solution is based on combining two passes using the first as reference: with both beams from the first pass (incident angle $\theta_{i1}=\theta_{i2}$) and one beam from the second pass (flight direction α_3, incident angle θ_{i3}). Equation (3) can be written as $\boldsymbol{u} = \mathbf{B}\,\boldsymbol{v}$. The solutions of the three surface velocity components are

$$v_x = \frac{D_{B1}}{D_B}; \quad v_y = \frac{D_{B2}}{D_B}; \quad v_z = \frac{D_{B3}}{D_B}, \tag{4}$$

where D_B is the determinant of matrix **B**, and D_{Bj} the determinant of the matrix formed by replacing the j-th column of **B** with vector $\boldsymbol{u}$. Further detail is given in [15]. For the wave spectral analysis, the surface velocity from 3D solution is used. Fig. 1 shows the maps of v_x, v_y and v_z measured by the DBI. The flow of the GS in this region is primarily northbound. From in situ current measurements, the daily average of the northbound velocity at the core of the GS is about 1.9 m/s, estimated from the contour map in Fig. 13b of [14]. The mean velocity of v_y displayed in Fig. 1 (middle panel) represents an instantaneous snapshot of the surface current over a sizable region (the length of overlap data is about 78 s, the area of coverage about 1.7 km × 7.8 km), the maximal magnitude is about 2 m/s. A strong gradient of v_y is clearly discernable. The velocity gradient near the GS front is about 1 m/s over a lateral distance of 500 m, corresponding to a strong velocity shear of 2×10^{-3} s^{-1}. The velocity contrast in v_x or v_z is much weaker and the boundary of the GS is barely discernable (top and bottom panels, Fig. 1).

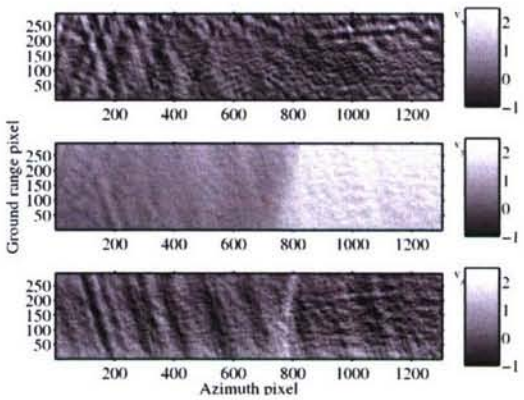

Figure 1. The maps of the surface velocity field, v_x, v_y and v_z.

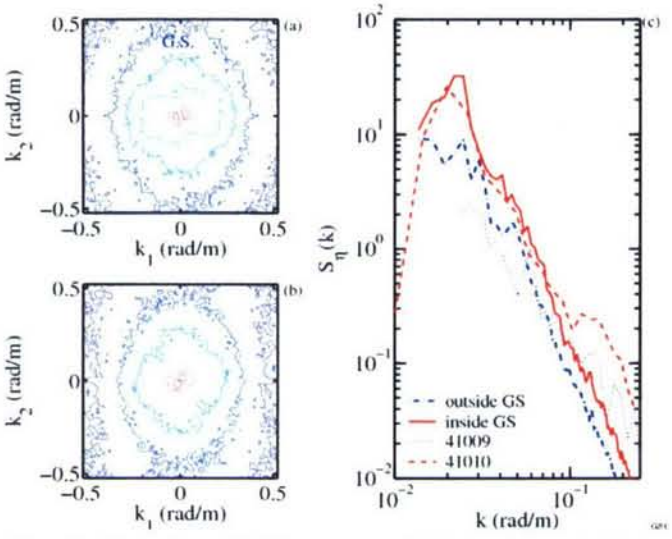

Figure 2. Comparison of the 2D wave spectra (a) inside and (b) outside the Gulf Stream, (c) 1D spectra from DBI and buoy measurements.

IV. Wave Spectral Analysis

With image data like Fig. 1, it is straightforward to compute the wave spectrum using the 2D fast Fourier transform (FFT). Wave properties derived from InSAR have been compared with in situ measurements obtained by a pressure gauge array in southern California [4-5]. The wind is low (2 m/s) and the wave field is swell dominated. The results show that the InSAR and buoy data are in very good agreement for waves propagating in the range direction and the quality of agreement deteriorates for waves traveling in the azimuth direction. Similar conclusion is reached in [7].

We have performed 2D spectral analysis for the DBI data using v_z derived from the 3D solution combining two flight passes through the same region (Fig. 1). The advantage of using v_z instead of v_x or v_y is that v_z does not dependent on the wave propagation direction and the conversion of velocity to displacement spectrum is simpler. Figs. 2a and 2b display the 2D velocity spectra, $S_v(k_x,k_y)$, inside and outside GS.

Poorer resolution in the azimuth direction due to the velocity bunching effect [9, 16] is clearly shown from the contours of the 2D spectra. The 2D spectra can be integrated to yield 1D spectra to compare with buoy measurements. As shown in Fig. 2c, the agreement of DBI spectrum inside the GS and the offshore buoy measurements (41010) is excellent when the effects of shoaling refraction and current modulation are taken into account. Just a couple of kilometers away in the inshore side of the current front, the waves are distinctively different in three respects. (a) The spectral density level is the GS is considerably higher, by about a factor of two. (b) The directional distribution of the wave spectral contours outside the GS is rotated counterclockwise by about 20 to 30 degrees in comparison with the spectrum inside the GS. And (c) there is a conspicuous crosshatched wave pattern in the dominant scale signal components in the GS side of the sharp current front. The last aspect is more visible through a signal decomposition analysis procedure described in [15]. The directional difference of the two wave fields is consistent with that expected from wave-current interaction. This can be described by the wave-number conservation equation [17]

$$\frac{\partial \boldsymbol{k}}{\partial t} + \nabla n = 0 , \tag{5}$$

where n is the apparent frequency of the wave field, which is related to the intrinsic frequency, ω, by $n=\omega+\boldsymbol{k}\cdot\boldsymbol{U}$ and $\boldsymbol{U}$ is the current vector. Assuming that the intrinsic frequency does not vary with space, the current field simplifies to $\boldsymbol{U}=(0, V)$, and $\partial/\partial y=0$, then (3) becomes

$$\begin{aligned} \frac{\partial k_1}{\partial t} &= -\frac{\partial (k_2 V)}{\partial x} \\ \frac{\partial k_2}{\partial t} &= 0 \end{aligned} . \tag{6}$$

Fig. 3 shows an example of the trajectories of wave trains with a southbound component going through a current field $V(x)= V_0\exp[-(x/x_b)^q]$, with V_0=2 m/s, q=8 and x_b=80 km. The evolution of wave propagation is consistent with the 2D wavenumber spectra shown in Fig. 2. As noted earlier, the wave variance inside the GS is about twice of that in the outside water. This is considerably higher than that expected from hydrodynamic modulation, calculated to be about 10 percent ($k=2\times10^{-2}$ rad/m) to 12 percent ($k=3\times10^{-2}$ rad/m) for the observed swell components. A more likely mechanism contributing to the observed intensification of the wave field inside the GS is the "wave guide" effect produced by the strong velocity gradient at the GS front. With the right combinations of the wave and current properties, waves can be trapped inside the GS. This effect occurs when the change of k_1 following (6) is so large that k_1 changes sign (reversing the propagation direction). The formation of a wave guide by a shear current is a delicate combination of several parameters including the velocity shear, the width of the current, the wavelength and the direction of wave propagation. As shown in Fig. 3, for $k=2\times10^{-2}$ rad/m, wave components propagating at angles close to ±20° are trapped inside the current. The spectral peak wavenumber of the wave field at the time of data collection is close to 2×10^{-2} rad/m and the source of the swell is from north and northeast. The wave guide effect may be important in producing the large enhancement of waves inside the GS in the present data set.

V. Summary

A DBI employs two sets of InSAR to acquire two radial velocity components in a single flight pass. In an earlier study, it was shown that the resolved surface velocity fields over barrier islands follow the expected outflow pattern of tidal flows [13]. In this paper, DBI data were acquired in the vicinity of the GS boundary. Combining two flight passes over the same region, all three orthogonal components of the surface velocity can be retrieved. The mean current field is in good agreement with in situ measurements reported in the literature [14]. The wave spectra computed from the DBI data are in good agreement with in situ buoy output. The difference in the propagation di-

rection of waves inside and outside the GS detected from the 2D wave spectra is consistent with the refraction effect expected from wave-current interaction. For the swell system is the present data set, the wave variance inside GS is about twice of that outside GS. The level of enhancement is considerably higher than that can be explained by the hydrodynamic modulation. Generation of waves by local wind is not an important factor judging from the long wave period and low wind speed, so is the stability effect and both factors can be ignored in this case. (Even when all three factors are important, earlier investigation indicates 25 to 50 percent wave variance enhancement by the Kuroshio using the Topex/Poseidon data [18].)

A more likely explanation of the excessive wave enhancement inside the GS in the present data set is that the GS can act as a wave guide and trap waves within the current boundaries when the right combinations of wave length, propagation direction, current width and shear level of the current field exist. Numerical computations suggest that the surface wave properties at the time of data acquisition may satisfy the selective conditions for wave trapping. The hypothesis is further supported by the appearance of standing wave (cross-hatched) pattern on the GS side of the velocity front, which is indicative of swell bouncing off the sharp current front as a result of wave trapping [15].

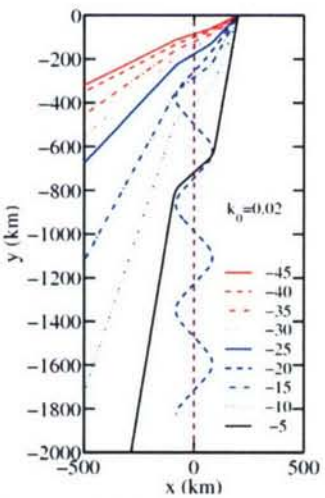

Figure 3. Numerical computations illustrating the wave trapping effect of the Gulf Stream wave guide.

ACKNOWLEDGMENT

This work is sponsored by the Office of Naval Research (NRL PE 61153 and 62435), NRL contribution PP/7330—06-6191.

REFERENCES

[1] Goldstein, R. M., and H. A. Zebker, Interferometric radar measurement of ocean surface currents, *Nature, 328*, 707-709, 1987.

[2] Goldstein, R. M., T. P. Barnett, and H. A. Zebker, Remote sensing of ocean currents, *Science, 246*, 1282-1285, 1989.

[3] Graber, H. C., D. R. Thompson, R. E. Carande, Ocean surface features and currents measured with synthetic aperture radar interferometry and HF radar, *J. Geophys. Res., 101*, 25813-25832, 1996.

[4] Marom, M., R. M. Goldstein, E. B. Thornton, and L. Shemer, Remote sensing of ocean wave spectra by interferometric synthetic aperture radar, *Nature, 345*, 793-795, 1990.

[5] Marom, M., L. Shemer, and E. B. Thornton, Energy density directional spectra of a nearshore wave field measured by interferometric synthetic aperture radar, *J. Geophys. Res., 96*, 22125-22134, 1991.

[6] Shemer, L., M. Marom, and D. Markman, Estimates of currents in the nearshore ocean region using interferometric synthetic aperture radar, *J. Geophys. Res., 98*, 7001-7010, 1993.

[7] Goldstein, R. M., F. Li, J. Smith, R. Pinkel, and T. P. Barnett, Remote sensing of ocean waves: The surface wave process program experiment, *J. Geophys. Res., 99*, 7945-7950, 1994.

[8] Alpers, W., and K. Hasselmann, The two-frequency microwave technique for measuring ocean-wave spectra from an airplane or satellite, *Bound.-Layer Meteorol., 13*, 215-230, 1978.

[9] Hasselmann, K., R. K. Raney, W. J. Plant, W. Alpers, R. A. Shuchman, D. R. Lyzenga, C. L. Rufenach, and M. J. Tucker, Theory of synthetic aperture radar ocean imaging: A MARSEN view, *J. Geophys. Res., 90*, 4659-4686, 1985.

[10] Rodriguez, E., D. Imel, and B. Houshmand, Two-dimensional surface wave currents using vector along-track interferometry, in *Proc. PIERS'95 Conf.*, Seattle, WA, 763, 1995.

[11] Frasier, S. J., and A. J. Camps, Dual-beam interferometry for ocean surface current vector mapping, *IEEE Trans. Geos. Rem. Sens., 39*, 401-414, 2001.

[12] Farquharson, G., W. J. Junek, R. Ramanathan, S. J. Frasier, R. Tessier, D. J. McLaughlin, M. A. Sletten, and J. V. Toporkov, A pod-based dual-beam SAR, *IEEE Geos. Rem. Sens. Lett., 1*, 62-65, 2004.

[13] Toporkov, J., D. Perkovic, G. Farquharson, M. A. Sletten, and S. J. Frasier, Sea surface velocity vector retrieval using dual-beam interferometry: First demonstration, *IEEE Trans. Geos. Rem. Sens., 43*, 2494-2502, 2005.

[14] Zantopp, R. J., K. D. Leaman, and T. N. Lee, Florida Current meanders: A close look in June-July 1984, *J. Phys. Oceanogr., 17*, 584-593, 1987.

[15] Hwang, P. A., J. V. Toporkov, M. A. Sletten, D. Lamb, and D. Perkovic, An experimental investigation of wave measurements using a dual-beam interferometer: Gulf Stream as a surface wave guide. Subm. *J. Geophys. Res.*, doi:10.1029/2006JC003482, 2006.

[16] Alpers, W. R., and C, L, Rufenach, The effect of orbital motions on synthetic aperture radar imagery of ocean waves, *IEEE Trans. Antennas Propagat., AP-27*, 685-690, 1979.

[17] Phillips, O. M., *The dynamics of the upper ocean*, 2nd ed., Cambridge Univ. Press, Cambridge, UK, 336 pp., 1977.

[18] Hwang, P. A., Altimeter measurements of the wind and wave modulation by the Kuroshio in the Yellow and East China Seas, *J. Oceanogr., 61*, 987-993, 2005.